Self-modulated laser-plasma acceleration in a H_2 gas target, simulated in a spectral particle-in-cell algorithm: wakefield and electron bunch properties

Edison Puig Maldonado
Instituto Tecnológico de Aeronáutica
São José dos Campos/SP, Brazil
puig@ita.br

Ricardo Elgul Samad
Instituto de Pesquisas Energéticas e Nucleares
São Paulo/SP, Brazil
resamad@gmail.com

Armando Valter Felicio Zuffi
Instituto de Pesquisas Energéticas e Nucleares
São Paulo/SP, Brazil
armandozuffi@gmail.com

Fabio Bittencourt Dutra Tabacow
Instituto de Pesquisas Energéticas e Nucleares
São Paulo/SP, Brazil
fabio.tabacow@gmail.com

Nilson Dias Vieira Junior
Instituto de Pesquisas Energéticas e Nucleares
São Paulo/SP, Brazil
nilsondiasvieirajr@gmail.com

***Abstract*—We evaluate the results of self-modulated, laser wakefield acceleration of electrons in homogeneous, 150-µm-thick hydrogen gas target, simulated using the spectral particle-in-cell algorithm FBPIC. Considering a single 2-TW laser pulse at 800-nm, which generates ionization and plasma displacement at relativistic intensities, we discuss the resultant wakefield phases, wave-breaking, and the ejected electron bunch properties: charge, length, divergence and energy, also comparing with experimental results.**

Keywords—Laser wakefield, laser-plasma acceleration, particle in cell (PIC), plasma simulation, particle beams simulation.

I. INTRODUCTION

Current techniques of laser wakefield acceleration, LWFA, allow generation of electron beams with kinetic energies in the MeV-GeV range, low divergence (<1 mrad) and small energy dispersion (few percent), electric charge on the pC-nC range, duration as short as 1 fs, and repetition rate in Hz-kHz range [1, 2]. The electron beams produced by LWFA, are typically composed by one or more electron bunches with subpicosecond duration, generated at each laser pulse shot, and this can be done periodically with the repetition rate now limited by the present laser technology. Using TW class tabletop laser systems, these novel electron beams are generated in more compact and cheaper accelerators than traditional RF technology, allowing many applications and new techniques [3, 4]. In LWFA, the plasma wave that carries the electrons can sustain longitudinal electric fields, E_z, stronger than 100 GV/m, well above the 100 MV/m typically found in conventional RF accelerators [5]. The interaction of these beams with matter allows the development of tunable, compact sources of high energy ionizing radiation [6], which are applied to new imaging techniques [7]. Other possible uses of laser particle accelerators are the production of isotopes for medicine [8, 9], protontherapy, hadron therapy [4, 10] and fast ignition in fusion targets [11, 12].

Different laser wakefield acceleration regimes and techniques exist [13, 14], but the underlying requirements are: (1) to focus an ultrashort (subpicosecond) laser pulse to intensities above 10^{17} W/cm^2 and propagate it over a length in the mm range of a tailored gas target; (2) to ionize the gas and excite a high-amplitude wakefield behind the laser pulse(s); (3) to receive extra electrons injected in this wakefield from the background of the main ionized-gas plasma or from other present ionizable species; (4) to maintain those extra electrons trapped in the wakefield, being accelerated by the intense local electrostatic field until they are finally ejected as a bunch of relativistic electrons in the laser propagation direction; (5) in some cases, further contribution to the acceleration by the Lorentz force, a form of direct laser acceleration, DLA, by the overlap of the laser pulse and the injected electrons [15].

The technology to create gas targets for laser-plasma phenomena is mainly composed of nozzles, ducts and cells. Gas nozzles are simple and versatile devices to create reproducible high-density, sonic and supersonic gas targets for laser-plasma experiments. For gas jets with high Mach numbers, sharp jet-vacuum boundaries and flat-top density profiles are typically obtained, simplifying design and analysis of laser-plasma experiments [16]. Various molecular and atomic gases have been successfully used in LWFA, H_2 He, Ar, N_2, among others, but hydrogen is convenient for its simplicity and has produced new and interesting recent results, as will be discussed in Section II.

Particle-in-cell (PIC) codes are known since the late 1950s and are widely used in plasma physics. They are the most employed tool for simulating laser-plasma dynamics [17]. In the last ten years, a new approach of relativistic PIC code was devised using spectral decomposition of EM fields, replacing the traditional finite-difference methods by solving the Maxwell equations in Fourier space. This is especially beneficial in cylindrical (coordinate system) algorithms, where, considering the general symmetry of the laser-plasma interaction, an azimuthal Fourier decomposition of the EM field components can typically reduce the cost of the simulation to a few times that of a 2D Cartesian simulation, instead that of a full 3D Cartesian simulation [18]. These codes generate results that are in total agreement with those of fully 3D simulations, therefore can be used in a less time-consuming mode. Additionally, unlike standard finite-difference PIC codes, they are free of the spurious numerical dispersion (in vacuum) effect, zero-order numerical Cherenkov effect and other numerical artifacts [19, 20].

I. PRINCIPLES OF LWFA

In laser wakefield acceleration (LWFA) systems, plasma is generated by field-induced ionization that typically occurs at intensities above 10^{14} W/cm^2. Those intensities must occur in the leading edge of the laser pulse, and the propagation and interaction of the remaining part of the pulse with the plasma is possible only if the density of the freed electrons is

This work was supported by FAPESP and CNPq grants.

978-1-7281-3092-7/19/$31.00 ©2019 IEEE

below a limiting value, the so-called critical density, $n_{cr} = \epsilon_0 m_e(\omega/e)^2$, where ϵ_0 is the vacuum permittivity, e is the elementary charge, m_e is the electron mass and ω is the laser frequency. If the plasma electrons are denser, the laser is fully reflected [21]. At the wavelength λ= 800 nm, the critical density is: $n_{cr} = 1.75 \times 10^{21}$ cm^{-3}. Typically, in a laser-generated underdense plasma, the laser pulse propagates without significant loss, displacing the charges by the ponderomotive force and possibly exciting an intense plasma wave in its wakefield [13]. When perturbed from the equilibrium by the pump laser, the fundamental response of a neutral plasma is to oscillate its electrons at the plasma frequency, $\omega_P = (e/\epsilon_0^{1/2}) \times (n_e/m_e)^{1/2}$, where n_e is the local, initial number density of electrons. Sometimes, the literature presents it as $\omega_P = (4\pi e) \times (n_e/m_e)^{1/2}$, in CGS units. In general, the optical properties of the laser-generated disturbed plasma are: (1) relativistic nonlinearity due to the quiver motion of electrons at a fraction of the speed of light, altering the electron mass and thus changing the local value of the plasma frequency; (2) perturbation of the plasma electronic density by the ponderomotive force, thus also changing the local value of the plasma frequency; (3) excitation of electronic waves, where the inertially frozen ions provide the restoring force.

The wavelength of the wakefield is that of a Langmuir wave, $\lambda_P \approx 2\pi c/\omega_P = (2\pi c/e) \times (\epsilon_0 m_e/n_e)^{1/2}$, where c is the speed of light in vacuum [20]. In fact, the plasma phase velocity is $v_{ph} = c / [1 - (\omega_P / \omega_0)^2]^{1/2}$, where ω_0 is the (pump or probe) laser frequency and the plasma group velocity for the laser pulse is $v_G = c \times [1 - (\omega_P / \omega_0)^2]^{1/2}$. The effects discussed in the preceding paragraph cause local modulations of the plasma local refractive index, $\eta_P = c / v_{ph}$ [3]. In general, the most significant mechanism for dissipation of laser energy is via collision between electrons and ions. Also, the laser pulse suffers some energy dissipation due to the ionization process, multi-photon absorption, ion motions and heat effects.

When describing the behavior and the various regimes of a laser-plasma accelerator, it is convenient to represent the electric field by a dimensionless parameter, the normalized laser amplitude at the peak of the laser pulse $a_0 = eA/m_e c$, where A is the vector potential of the electric field. For linearly-polarized laser, $a_0 \approx 8.6 \times 10^{-10} (I_L \lambda_L^2)^{1/2}$, where λ_L is the laser wavelength in μm and I_L is the laser pulse peak intensity in W/cm^2 [14], This parameter is also often called normalized vector potential, normalized laser strength parameter, or normalized momentum. This description of the laser field is useful since the quiver motion of plasma electrons becomes relativistic when $a_0 = 1$. For $a_0 > 1$, the relativistic increase in the electron mass decreases the plasma frequency and this increases the wavelength of the plasma wave, thus causing a saw-tooth-like profile in the laser wakefield longitudinal-cut cross section, what is called a *nonlinear wakefield* [13]. For laser pulses with $\lambda = 0.8$ μm, relativistic electron displacement occurs for peak intensities of approximately 2×10^{18} Wcm^{-2}.

Homogeneous gas targets have specific values of atomic number density. If the laser pulse saturates all possible ionizations across the transverse profile of such target, the resultant freed electron density is predictable and approximately constant. Therefore, this homogeneous plasma in the beam path manifests a specific plasma wavelength. When a laser pulse length is shorter than this wavelength, $L_0 = c\tau_0/\eta \leq \lambda_P$, where τ_0 is the initial pulse duration FWHM, the excitation of the laser-plasma wakefield is accomplished at the *direct resonant* regime. If the laser has both transverse (waist w_0) and longitudinal (pulse length L_0) dimensions around or smaller than λ_P, the laser pulse can even drive a nonlinear wakefield with near spherical cavities [2]. If injected electrons are trapped and accelerated in this resonant laser wakefield, it is usual to refer to it as the *blowout*, or *bubble*, regime of laser wakefield acceleration, simply LWFA. To provide those additional injected electrons, one must use externally pre-accelerated electrons, ionization injection by using a mixture of gases or exploit the effect of self-injection due to a longitudinal or transversal wave break. For wave-breaking, the normalized laser amplitude at the peak of the laser pulse must be [22]:

$$a_0 > (2\,\omega/\omega_p)^{2/3} \quad (1)$$

To operate LWFA (resonantly) in the blowout regime, it is expected that the laser peak power, P_L, is higher than the critical power: $P_c^{bubble} \approx 30\ (\tau_0\,[\text{fs}] / \lambda_L\,[\mu\text{m}])^2$ GW [23]. As an example, if $\tau_0 = 50$ fs and $\lambda_L = 0.8$ μm, $P_c^{bubble} \approx 120$ TW.

The main scaling limitations of LWFA are evaluated defining two characteristic lengths: the pump depletion length $L_{pd} = \lambda_P^3/\lambda_L^2$, estimated by equating the laser pulse energy to the energy left behind in the wakefield; also, the electron dephasing, or outrunning the plasma wave, can limit the energy gain in the wakefield to a dephasing length [13]:

$$L_d = \lambda_P^3/2\lambda_L^2 \quad (2)$$

II. Principles of SM-LWFA

Under appropriate conditions, it is possible for a laser pulse much longer than the plasma wavelength (as well as without transverse matching dimensions) to drive an intense wakefield when it is strongly self-modulated by the initial plasma instabilities, such that its amplitude envelope becomes progressively modulated with periodicity λ_P. Physically, self-modulation occurs because the plasma wave produces periodic focusing and defocusing local effects that, combined with diffraction, modulates the beam. After being modulated, the laser pulse, now a pulse train, drives a stronger plasma wakefield, and the process intensifies each step. When such large wakefield receives injected electrons and accelerates them, the mechanism is known as self-modulated laser wakefield acceleration, SM-LWFA [24].

This mechanism is often used when available laser pulses have an initial normalized laser amplitude $a_0 \leq 1$. This is the case of the contemporary kHz-repetition-rate chirped-pulse-amplifiers (CPA), typically with sub-terawatt (TW) laser pulses, energy < 30 mJ and duration > 30 fs.

The first experimental high-repetition-rate SM-LWFA was demonstrated in 2013 using < 10 mJ, 30 fs laser pulses and a 100 μm gas target [25]. Generation of accelerated electron bunches with charges up to ~ 0.5 nC and energies ~ 1 MeV was demonstrated in 2015 using sub-terawatt laser pulses (50 fs, 10–50 mJ) in a hydrogen gas jet with a density above 10^{20} cm^{-3} and ~200 μm thickness [26]. In 2017, electron acceleration at 1 kHz with ~10 mJ laser pulses was experimentally realized using hydrogen gas jets with (non-uniform) densities > 10^{20} cm^{-3}, generating bunches with ~1 pC charge and ~1 MeV energy [27]. The same research group demonstrated in 2018 the acceleration of electron bunches exhibiting ~1 nC and ~1 MeV by using laser wavelength of 3.9 μm with 100-fs, 0.25-TW pulses at 20 Hz, in a 150 μm hydrogen gas jet [28]. When the incident laser pulse normalized amplitude, a_0 , is insufficient to drive a nonlinear wakefield but its peak power at least exceeds the

critical power for relativistic self-focusing in the plasma, $P_c = 17\ (\omega_0/\omega_p)^2 = 17\ (n_{cr}/n_e)$ GW, the laser pulse will evolve to a new spot size of the order of the laser wavelength. At this new value of normalized laser amplitude, a_0', 2-5 times the initial a_0, both the threshold for nonlinear wakefield and for wave break can be reached, and self-injected wakefield acceleration occurs [13]. As an example, to surpass the critical power for self-focusing, gas targets that allow plasma densities $n_e > 3 \times 10^{19}$ cm^{-3} must be used for 1 TW laser pulses. In fact, sub-TW SM-LWFA typically must be operated at plasma densities $n_e > 10^{20}$ cm^{-3} to fulfill the requirement of self-focusing. However, the density must be chosen carefully since for $P_L / P_c \geq 4$ the induced filament can rapidly disintegrate the laser field envelope and violate the process of exciting a plasma wave. Moreover, it has been shown that for < 0.25-TW pulses, degradation of LWFA performance occurs, which cannot be recovered by adjusting the density of the gas target [23].

III. Methods

We decided to use a spectral and cylindrical PIC code, taking advantage of the symmetry of the problem, reducing computing requirements. We used FBPIC, Fourier-Bessel Particle-In-Cell, from Lawrence Berkeley National Lab and CFEL, Hamburg University. This tool uses analytical integration in spectral space (not presenting finite-difference artifacts), centering in time and space (not presenting interpolation artifacts) and a cylindrical grid with azimuthal decomposition (consuming less memory and time than 3D Cartesian codes). The density of free electrons is calculated with the Ammosov–Delone–Krainov (ADK) model [29].

TABLE 1 – PHYSICAL LASER PARAMETERS USED IN SIMULATION

PARAMETER	VALUE
WAVELENGTH, λ_L [μm]	0.8
LASER_W0, w_0 [μm]	4
PULSE_ENERGY, ε [mJ]	100
PULSE_DURATION, Δt [fs]	50
Z_FOC [μm]	50

TABLE 2 – RELEVANT QUANTITIES CALCULATED FROM TABLE 1

QUANTITY	VALUE
PLASMA GROUP VELOCITY [v_G / c]	0.94
BEAMWAIST AREA, A [cm²]	4.8
CONFOCAL PARAMETER, b [μm]	120
PEAK POWER, PP [TW]	2
LASER INTENSITY [10^{18} W cm^{-2}]	4.3
PULSE LENGTH [μm]	15
PLASMA WAVELENGTH [μm]	2.4
LASER A0	1.4
DEPHASING LENGTH [μm]	10
ESTIMATED SELF-FOCUSED LASER A0	5.5
WAVE BREAK LIMIT FOR A0	3.3

TABLE 3 – SIMULATION PARAMETERS

SIMULATION PARAMETER	VALUE
LENGTH OF THE SIMULATION BOX [μm]	50
SIMULATION BOX RADIUS [μm]	30
NUMBER OF GRID POINTS ALONG Z (× 1000)	1.9
NUMBER OF GRID POINTS ALONG R (× 1000)	0.6
NUMBER OF AZIMUTHAL MODES, N_m	4
SPEED OF THE MOVING WINDOW [c]	0.9
SIMULATION LENGTH [μm]	300
SIMULATION TIMESTEP [as]	89
PERIOD OF DIAGNOSTICS [TIMESTEPS]	500

The simulated setup is composed by a laser at the wavelength λ_L = 800 nm, propagating in the z-direction, linearly polarized in the x-direction. The target gas is neutral H_2 in a 140 μm thick flow, with entry and exit density ramps assumed 10 μm wide. The density profile is shown in Fig. 1, where, z_1 = 10 μm, z_2 = 20 μm, z_3 = 150 μm and z_4 = 160 μm. The number density of H atoms at the top is 2×10^{20} cm^{-3}. Outside this profile it is assumed that the background in the experimental chamber is below 10^{14} cm^{-3}. The laser parameters in this study are displayed in Table 1: wavelength, beam waist in vacuum, pulse energy, pulse duration and position of laser focus in vacuum (Z_FOC). Therefore, we can calculate other relevant quantities, as shown in Table 2, listed here with an arbitrary choice of significant digits. In this table, the necessary a_0 for wave breaking is calculated using (1), the laser pulse a_0' after self-focusing, evaluated assuming a new beam waist of 1 μm, as well as the calculated dephasing length using (2). The configuration of the simulation is shown by the parameters shown in Table 3. The number of grid points was defined accordingly the UCLA criteria [30] and the number of azimuthal modes, N_m, higher than recommended to represent non-linear effects [31, 20]. We used the openPMD Viewer, from Lawrence Berkeley National Laboratory for quick inspection of simulation results. Further analyses were performed using Mathematica 12.

IV. Results

A. Laser electric field and plasma wakefield

After propagating just ~25 μm in the region with homogeneous density, the laser pulse suffers relativistic self-focusing to new spot size, as shown in Fig. 2 for a later iteration, at 132 fs. As can be seen from the figure, the electric field reaches a value 1.5×10^{13} V/m, or normalized laser amplitude a_0' = 4.7, corresponding to a new spot size of 1.2 μm. The longitudinal current density field immediately after the self-focusing of the laser pulse is shown in Fig. 3. It can be observed the onset of a wakefield, with two or three periods at the plasma wavelength (at $z \sim 70$ μm). Also, one can see a significant stream of background electrons grouped near the axis, exhibiting a fine structure with periodicity of half the laser wavelength (inset), pushed by the Lorentz force combined with quiver motion. The plot of laser electric field in the same timestep is shown in the bottom half, already exhibiting some auto modulation at the plasma wavelength. Even before the final edge of the plasma, a first major wave break occurs at $z \approx 100$ μm, as can be seen in Fig. 4, with macroparticles surpassing the wakefield.

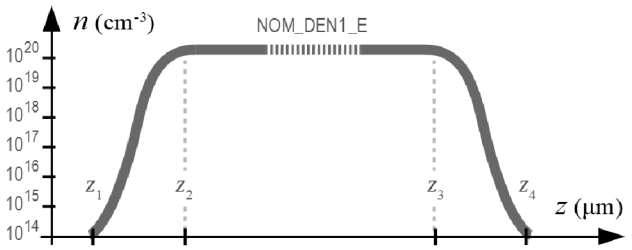

Fig. 1 – Gas density profile considered in this simulation. The entry ramp start is z_1 = 10 μm; the flat density start is z_2 = 20 μm; the exit ramp start is z_3 = 150 μm; the exit ramp end is z_4 = 170 μm.

Near the exiting edge of the designed plasma region, as seen in the current density J_z graph shown in Fig. 5, it is possible to characterize a wakefield, here with ten periods. A second major wave break occurs at the end of the plasma, or 160 μm, as seen in Fig. 6, and causes ejection of many macroparticles: the electronic bunch.

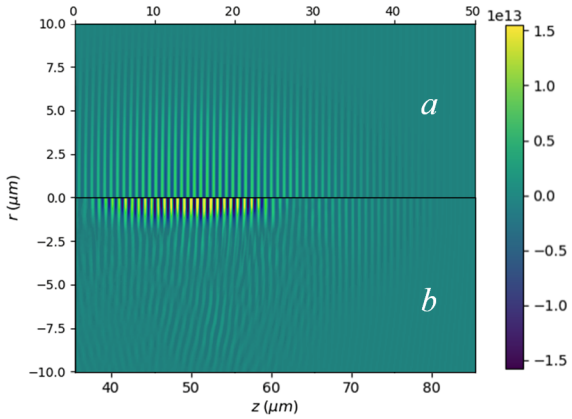

Fig. 2 – Laser pulse electric field (*x*-axis), in V/m, (a) at the beginning of the simulation (iteration 0) and (b) after self-focusing (iteration 1500).

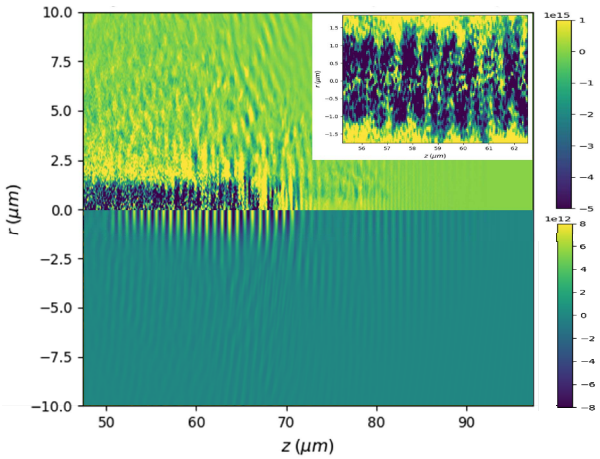

Fig. 3 – (Top) Snapshot of the *z*-axis current density, in A/m^2 at 176 fs (iteration 2000); (bottom) *x*-axis laser electric field (V/m). In the inset, zoom highlighting effects of Lorentz-force and quiver motion.

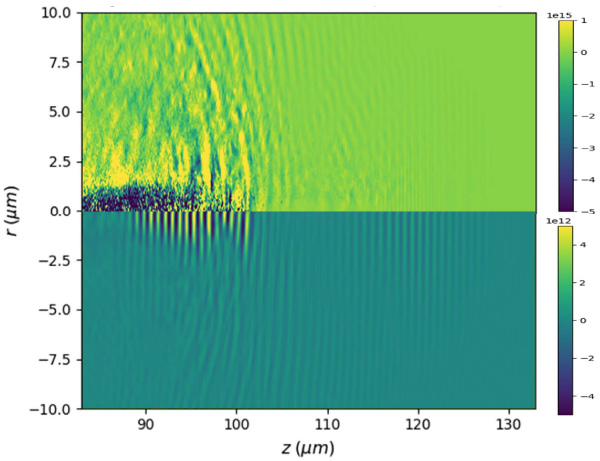

Fig. 4 – (Top) Snapshot of the *z*-axis current density, in A/m^2 at 307 fs (iteration 3500); (bottom) *x*-axis laser electric field (V/m).

B. *Electron bunch analysis*

Integrating the data, the radial direction provides the current distribution along the *z*-direction, shown in Fig. 6-a. The bunch was considered to be formed by the electrons outside the gas jet, shown in dark blue; its position was calculated as the first momentum of the distribution, shown as a black vertical line in Fig. 6-b, and its duration (shown as a shaded region) was considered to be twice the square root of its second momentum (variance), whose calculated value is 12.6 μm, corresponding to 42 fs. The same procedure was applied to the transversal direction, Fig. 6-c, providing a bunch width of 22.8 μm.

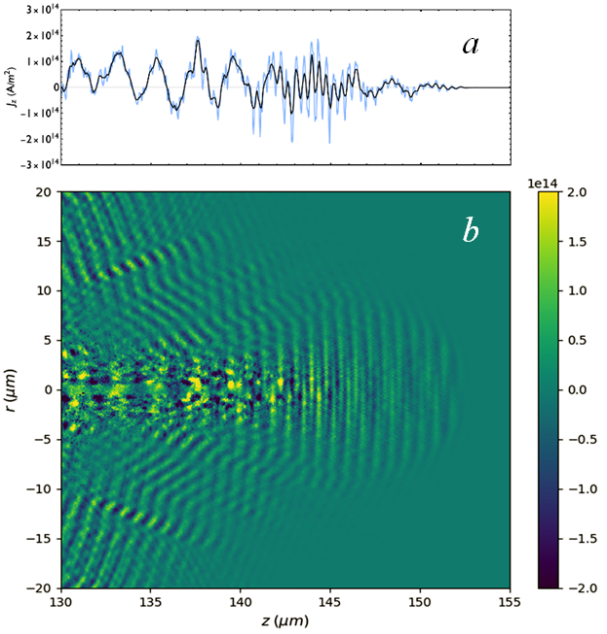

Fig. 5 – Snapshot of the *z*-axis current density at 395 fs (iteration 4500), with emphasis in the formed wakefield: (a) axis values and (b) color map.

FBPIC (fulfilling the openPMD standard) records a set of very useful matrices with physical properties of the particles (electrons), for each data dump. By using this data, it was possible to calculate the total electric charge of the bunch just after the bunch complete ejection: $q_{bunch}^{(7000)} \approx 1.84$ nC. Fig. 7 shows the *z*-momentum distribution at iterations 7000, 10000 and 14000, with calculated medians. Note that, as the bunch evolves in time, the median value shifts to higher values and more electrons assume higher momentum values.

We define for our study a bunch characteristic energy K_z, calculated using the median momentum, $\tilde{u}_z$, and relativistic energy–momentum relation, in MeV:

$$K_z = 0.51 \cdot ((\tilde{u}_z^2 + 1)^{1/2} - 1) \qquad (3)$$

The bunch characteristic energy after leaving the gas is 1.00 MeV, then increasing to 1.56 MeV after propagating the following 75 μm, and 1.93 MeV after an additional 100 μm.

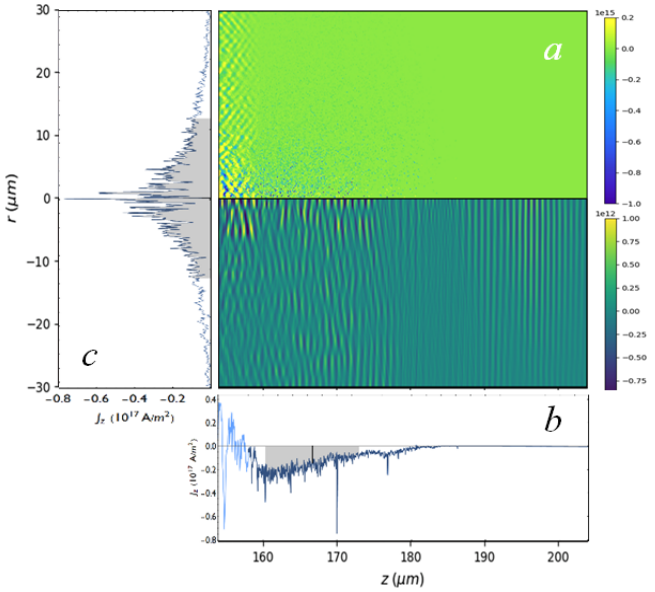

Fig. 6 – (a) (Top) Snapshot of the *z*-axis current density, in A/m^2 at 571 fs (iteration 6500); (bottom) *x*-axis laser electric field (V/m); (b) *z*-distribution and (c) *r*-distribution of the ejected macroparticles.

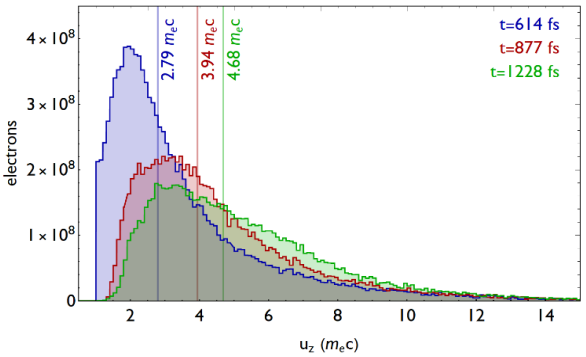

Fig. 7 – Snapshot of the z-momentum distribution, in $m_e c$ units, at three different times, 614 fs (when the bunch leaves the plasma), 877 fs and 1228 fs (185 µm after leaving the gas). The vertical lines are median values.

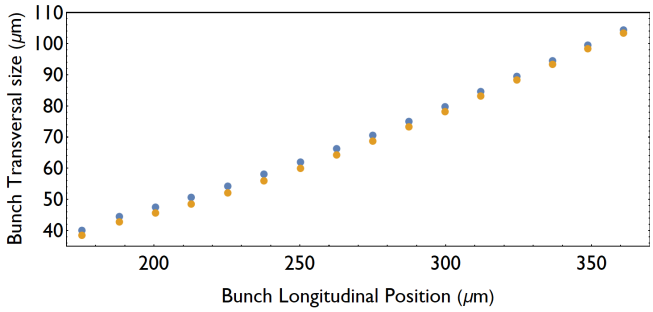

Fig. 8 – Electron bunch full transversal size in the x (blue) and y (orange) directions as a function of the bunch position.

The bunch z position was obtained as the first momentum of its z-distribution. The second central momenta of the x and y-distributions leaded to the sizes shown in Fig. 8. The found electron beam divergence is 347 mrad FWHM, a result in accordance with the expected for SM-LWFA regime [23, 26, 27] and 3-5 times larger than those from typical single-cycle, high-repetition rate, resonant LWFA systems [2].

V. Discussion

The results have agreed, in each step, with those typical reported in the recent literature, but the bunch energy behavior after the plasma indicate possible DLA in vacuum. This phenomenon is presently under study.

Nevertheless, our simulations revealed that, a TW-level laser pulse can produce, in a self modulated regime and with the proper gas density approaching (>10%) the critical density, a reasonable amount of electrons (in the nC range), with MeV energy, quite well collimated, making it suitable for practical applications.

Acknowledgment

We would like the thank Prof. Sudeep Banerjee of University of Nebraska, Lincoln, for helpful discussions. F. B. D. T. and A. V. F. Z. thanks CNPq for the scholarship.

References

1 V. Malka, "Laser plasma accelerators," *Phys. Plasmas*, vol. 19, no. 5, p. 055501, May 2012.

2 J. Faure et al., "A review of recent progress on laser-plasma acceleration at kHz repetition rate," *Plasma Phys. Control. Fusion*, vol. 61, no. 1, p. 014012, Jan. 2019.

3 T. Tajima, K. Nakajima, and G. Mourou, "Laser Acceleration," *Riv. del Nuovo Cim.*, vol. 40, no. 2, pp. 33–133, 2017.

4 A. Giulietti, *Laser-Driven Particle Acceleration Towards Radiobiology and Medicine*. Cham: Springer International Publishing, 2016.

5 V. Malka, "Plasma Wake Accelerators: Introduction and Historical Overview," *Cern Yellow Rep.*, vol. CERN-2016-, pp. 1–28, 2016.

6 K. T. Phuoc et al., "Laser based synchrotron radiation," *Phys. Plasmas*, vol. 12, no. 2, p. 023101, 2005.

7 F. Albert, "Next-Generation Light Sources: Laser Wakefield Accelerators," *Opt. Photonics News*, no. January, pp. 42–49, 2018.

8 K. Nemoto et al., "Laser-triggered ion acceleration and table top isotope production," *Appl. Phys. Lett.*, vol. 78, no. 5, pp. 595–597, 2001.

9 I. Spencer et al., "Laser generation of proton beams for the production of short-lived positron emitting radioisotopes," *Nucl. Instruments Methods Phys. Res. Sect. B Beam Interact. with Mater. Atoms*, vol. 183, no. 3–4, pp. 449–458, 2001.

10 K. Ledingham, P. Bolton, N. Shikazono, and C.-M. Ma, "Towards Laser Driven Hadron Cancer Radiotherapy: A Review of Progress," *Appl. Sci.*, vol. 4, no. 3, pp. 402–443, 2014.

11 H. Daido, M. Nishiuchi, and A. S. Pirozhkov, "Review of laser-driven ion sources and their applications," *Reports Prog. Phys.*, vol. 75, no. 5, 2012.

12 A. Macchi, M. Borghesi, and M. Passoni, "Ion acceleration by superintense laser-plasma interaction," *Rev. Mod. Phys.*, vol. 85, no. 2, pp. 751–793, 2013.

13 E. Esarey, C. B. Schroeder, and W. P. Leemans, "Physics of laser-driven plasma-based electron accelerators," *Rev. Mod. Phys.*, vol. 81, no. 3, pp. 1229–1285, 2009.

14 S. M. Hooker, "Developments in laser-driven plasma accelerators," *Nat. Photonics*, vol. 7, no. 10, pp. 775–782, 2013.

15 J. L. Shaw et al., "Role of direct laser acceleration in energy gained by electrons in a laser wakefield accelerator with ionization injection," *Plasma Phys. Control. Fusion*, vol. 56, no. 8, 2014.

16 K. Schmid and L. Veisz, "Supersonic gas jets for laser-plasma experiments," *Rev. Sci. Instrum.*, vol. 83, no. 5, 2012.

17 T. D. Arber et al., "Contemporary particle-in-cell approach to laser-plasma modelling," in *Plasma Physics and Controlled Fusion*, 2015, vol. 57, no. 11, pp. 1–26.

18 A. F. Lifschitz, X. Davoine, E. Lefebvre, J. Faure, C. Rechatin, and V. Malka, "Particle-in-Cell modelling of laser-plasma interaction using Fourier decomposition," *J. Comput. Phys.*, vol. 228, no. 5, pp. 1803–1814, 2009.

19 R. Lehe, M. Kirchen, I. A. Andriyash, B. B. Godfrey, and J. L. Vay, "A spectral, quasi-cylindrical and dispersion-free Particle-In-Cell algorithm," *Comput. Phys. Commun.*, vol. 203, pp. 66–82, 2016.

20 H. Vincenti *et al.*, "Accurate modeling of plasma acceleration with arbitrary order pseudo-spectral particle-in-cell methods," *Phys. Plasmas*, vol. 24, no. 3, p. 033115, 2017.

21 P. Mulser and D. Bauer, *High Power Laser-Matter Interaction*, vol. 238. Berlin, Heidelberg: Springer Berlin Heidelberg, 2010.

22 S. V. Bulanov et al., "Electron bunch acceleration in the wake wave breaking regime," *Plasma Phys. Reports*, vol. 32, no. 4, pp. 263–281, 2006.

23 C.-Y. Hsieh, M.-W. Lin, and S.-H. Chen, "Simulation study of the sub-terawatt laser wakefield acceleration operated in self-modulated regime," Phys. Plasmas, vol. 25, no. 2, p. 023101, Feb. 2018.

24 S. Y. Chen, M. Krishnan, A. Maksimchuk, R. Wagner, and D. Umstadter, "Detailed dynamics of electron beams self-trapped and accelerated in a self-modulated laser wakefield," *Phys. Plasmas*, vol. 6, no. 12, pp. 4739–4749, 1999.

25 Z. H. He et al., "High repetition-rate wakefield electron source generated by few-millijoule, 30 fs laser pulses on a density downramp," *New J. Phys.*, vol. 15, 2013.

26 A. J. Goers *et al.*, "Multi-MeV Electron Acceleration by Subterawatt Laser Pulses," *Phys. Rev. Lett.*, vol. 115, no. 19, pp. 1–5, 2015.

27 F. Salehi *et al.*, "MeV electron acceleration at 1 kHz with <10 mJ laser pulses," *Opt. Lett.*, vol. 42, no. 2, p. 215, Jan. 2017.

28 D. Woodbury *et al.*, "Laser wakefield acceleration with mid-IR laser pulses," *Opt. Lett.*, vol. 43, no. 5, p. 1131, Mar. 2018.

29 M. V. Ammosov, N. B. Delone, and V. P. Krainov, "Tunnel ionization of complex atoms and of atomic ions in an alternating electromagnetic field," *Sov. Phys. JETP*, vol. 64, no. December 1986, pp. 1191–1194, 1986.

30 J. L. Shaw, N. Lemos, K. A. Marsh, F. S. Tsung, W. B. Mori, and C. Joshi, "Estimation of direct laser acceleration in laser wakefield accelerators using particle-in-cell simulations," *Plasma Phys. Control. Fusion*, vol. 58, no. 3, p. 034008, Mar. 2016.

31 FBPIC contributors, 'FBPIC algorithm & features', 2016. [Online]. Available: fbpic.github.io/overview/pic_algorithm.html [Accessed: 29-May-2019].